ARTICLES

Widespread transcription at neuronal activity-regulated enhancers

Tae-Kyung Kim[1]*†, Martin Hemberg[2]*, Jesse M. Gray[1]*, Allen M. Costa[1], Daniel M. Bear[1], Jing Wu[3], David A. Harmin[1,4], Mike Laptewicz[1], Kellie Barbara-Haley[5], Scott Kuersten[6], Eirene Markenscoff-Papadimitriou[1]†, Dietmar Kuhl[7], Haruhiko Bito[8], Paul F. Worley[3], Gabriel Kreiman[2] & Michael E. Greenberg[1]

We used genome-wide sequencing methods to study stimulus-dependent enhancer function in mouse cortical neurons. We identified ~12,000 neuronal activity-regulated enhancers that are bound by the general transcriptional co-activator CBP in an activity-dependent manner. A function of CBP at enhancers may be to recruit RNA polymerase II (RNAPII), as we also observed activity-regulated RNAPII binding to thousands of enhancers. Notably, RNAPII at enhancers transcribes bi-directionally a novel class of enhancer RNAs (eRNAs) within enhancer domains defined by the presence of histone H3 monomethylated at lysine 4. The level of eRNA expression at neuronal enhancers positively correlates with the level of messenger RNA synthesis at nearby genes, suggesting that eRNA synthesis occurs specifically at enhancers that are actively engaged in promoting mRNA synthesis. These findings reveal that a widespread mechanism of enhancer activation involves RNAPII binding and eRNA synthesis.

During development and in mature organisms, cells respond to changes in their environment in part through changes in gene expression. Extracellular factors including growth factors, hormones and neurotransmitters activate programs of new gene expression in a manner that is temporally and spatially controlled by the coordinated action of *trans*-acting transcription factors that bind to *cis*-acting DNA regulatory elements including enhancers, insulators and promoters. Most studies of the mechanisms by which gene expression is induced in response to extracellular stimuli have focused on promoters, which lie adjacent to the site at which mRNA synthesis is initiated. In contrast, the mechanisms by which enhancers[1], which lie far away from the start site of mRNA synthesis, contribute to stimulus-dependent gene expression are not well characterized. In the nervous system, hundreds of genes are induced in response to sensory experience-dependent neuronal activation[2]. Exposure of primary neuronal cultures to an elevated level of potassium chloride (KCl) leads to membrane depolarization and an influx of calcium through L-type voltage-sensitive calcium channels[2]. The resulting increase in intracellular calcium level then triggers several calcium-dependent signalling pathways that ultimately lead to changes in gene expression. We used this *in vitro* neuronal culture system to characterize neuronal activity-regulated enhancers.

Defining activity-regulated enhancers

Recent genome-wide studies have established that enhancers can be defined as DNA sequences that bind the transcriptional co-activator p300/CBP, that bind histone H3 monomethylated at lysine 4 (H3K4me1), and that are located distally from known transcription start sites (TSSs)[3–5]. We applied these criteria to define neuronal activity-regulated enhancers. Using ChIP-Seq[6], we first identified CBP binding sites throughout the mouse genome using two different antibodies against CBP and selected only those CBP-bound genomic loci detected by both antibodies (Methods). We found that CBP binding genome-wide is markedly increased upon membrane depolarization (Figs 1, 2, middle, and Supplementary Figs 1e, 2 and 3). Before stimulation, we detected fewer than 1,000 CBP binding sites, whereas upon membrane depolarization we detected ~28,000 CBP binding sites (Methods). Of the CBP sites detected upon membrane depolarization, ~25,000 were at least 1 kilobase (kb) distal to known TSSs, suggesting that most activity-dependent CBP binding does not occur at promoters. To identify specifically CBP binding sites at enhancers, we asked which of the distal CBP sites are also bound by H3K4me1-modified histones, which mark active chromatin regions including enhancers[3,7,8]. About 13,000 distal CBP sites are located within 2 kb of H3K4me1-modified regions (Figs 1, 2b and Supplementary Figs 1c and 3). We removed from this enhancer list a subset (7%) of enhancers that in addition to binding H3K4me1 also bind the transcription-initiation-site-associated histone mark H3K4me3 (refs 7, 8) and therefore may represent uncharacterized promoters (Figs 1, 2, top, and Supplementary Figs 1c, 3 and 8a). We defined the remaining ~12,000 genomic loci where distal CBP sites are flanked by H3K4me1 as neuronal enhancers (see Methods for detailed description of enhancer definition). Approximately half of the neuronal enhancers have evolutionarily conserved sequences in the region of CBP binding, indicating that these enhancers are functionally important (Fig. 1 and Supplementary Fig. 1a, b).

The strong inducibility of CBP binding at thousands of neuronal enhancers and their presence near activity-regulated genes (for

[1]Department of Neurobiology, Harvard Medical School, 220 Longwood Avenue, Boston, Massachusetts 02115, USA. [2]Department of Ophthalmology, Children's Hospital Boston, Center for Brain Science and Swartz Center for Theoretical Neuroscience, Harvard University, 300 Longwood Avenue, Boston, Massachusetts 02115, USA. [3]The Solomon H. Snyder Department of Neuroscience, Johns Hopkins University School of Medicine, 725 North Wolfe Street, Baltimore, Maryland 21205, USA. [4]Children's Hospital Informatics Program at the Harvard-MIT Division of Health Sciences and Technology, 300 Longwood Avenue, Boston, Massachusetts 02115, USA. [5]Molecular Genetics Core facility, Children's Hospital Boston, 300 Longwood Avenue, Boston, Massachusetts 02115, USA. [6]Epicentre Biotechnologies, 726 Post Road, Madison, Wisconsin 53713, USA. [7]Institute for Molecular and Cellular Cognition (IMCC), Center for Molecular Neurobiology (ZMNH), University Medical Center Hamburg-Eppendorf (UKE), Falkenried 94, 20251 Hamburg, Germany. [8]Department of Neurochemistry, Graduate School of Medicine, University of Tokyo, Bunkyo-ku, Tokyo 113-0033, Japan. †Present addresses: University of Texas Southwestern Medical Center, Department of Neuroscience, 5323 Harry Hines Blvd, Dallas, Texas 75390-9111, USA (T.-K.K.); Graduate Program in Neuroscience, University of California San Francisco, 1550 4th Street, San Francisco, California 94158, USA (E.M.-P.).
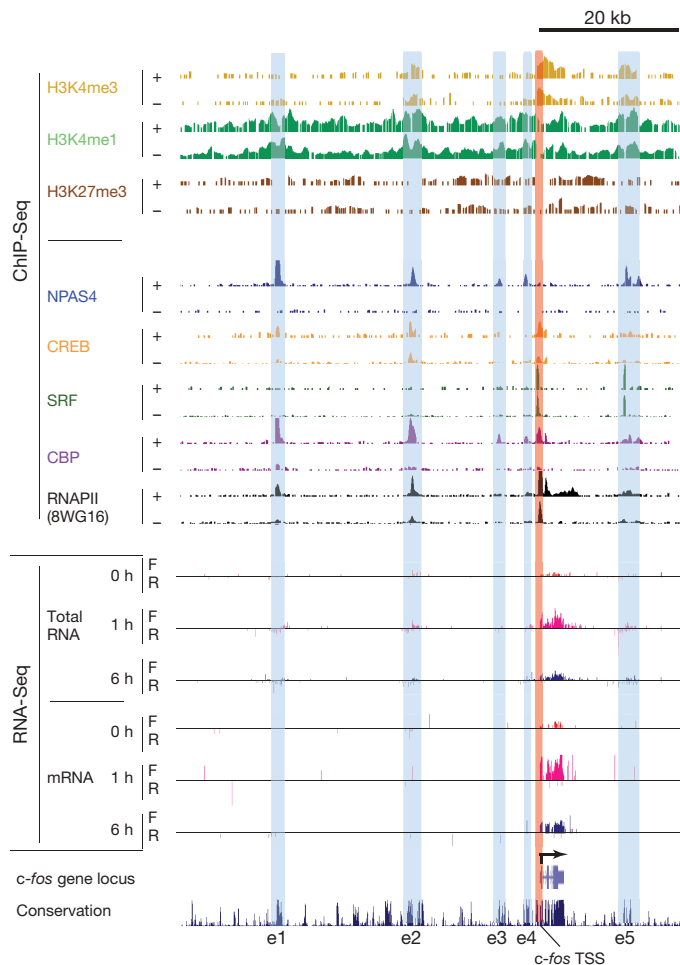*These authors contributed equally to this work.

Figure 1 | Enhancers near the *c-fos* gene with increased CBP/RNAPII/ NPAS4 binding and eRNA production upon membrane depolarization. ChIP-Seq: for each histone modification or transcription factor, two horizontal rows display the numbers of input-normalized ChIP-Seq reads across the locus, with '+' and '−' denoting the membrane-depolarized (2 h KCl) and unstimulated conditions, respectively. RNA-Seq: for each of 0, 1, or 6 h of membrane depolarization, the numbers of reads aligning to forward (F) and reverse (R) genomic strands are separately displayed. Enhancers identified in this study are highlighted by light-blue vertical bars (e1–e5), and the promoter region of c-fos gene is shown by a vertical light-red bar.

example, c-*fos*, *Rgs2* and *Nr4a2*) (Figs 1, 2b, middle, and Supplementary Table 2) indicate that these enhancers may contribute to the induction of activity-regulated gene expression. One activity-regulated neuronal enhancer was independently identified as an enhancer that drives the activity-regulated transcription of *Arc* (also called *arg3.1*), a gene that regulates synaptic function[9–12]. This *Arc* enhancer, which is located 7 kb upstream of the *Arc* TSS, is necessary to drive activity-regulated *Arc* transcription[13,14]. To determine if the activity-regulated enhancers we identified have the ability to induce transcription at a promoter in an activity-dependent manner, we tested seven of the enhancers in a luciferase reporter assay (Fig. 3). We found that six out of seven enhancers were able to induce expression of luciferase in an activity-dependent manner. Consistent with the known properties of enhancers, the induction of luciferase expression required the presence of an intact promoter.

Characterization of enhancers

We next asked what properties of the enhancers in addition to CBP binding change dynamically when neurons are exposed to a stimulus that triggers activity-regulated gene transcription. H3K4me1 shows a bi-modal pattern of binding that spans a 2–4-kb region with CBP binding at its centre. We defined these H3K4me1-binding regions
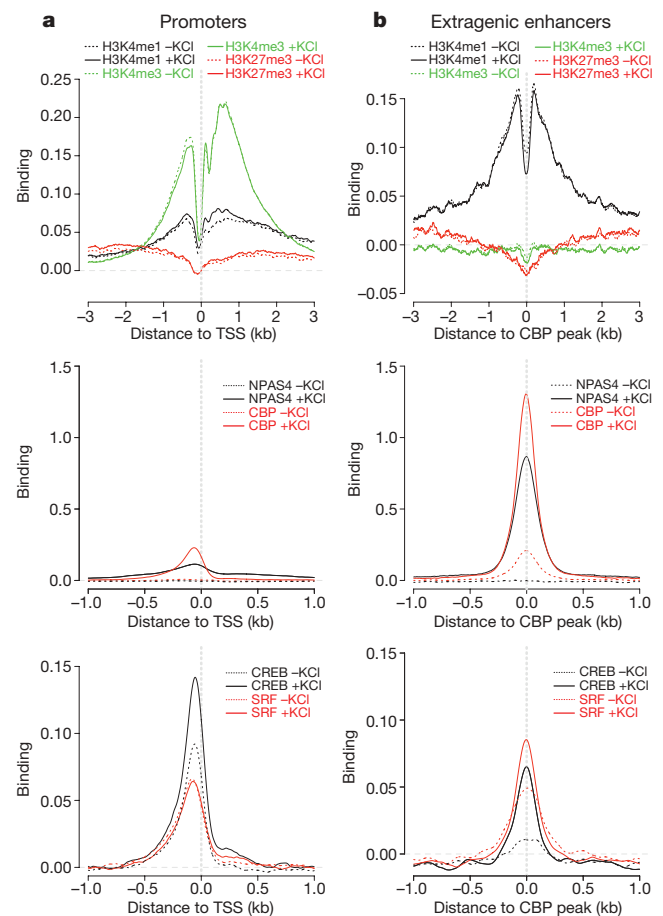

Figure 2 | Comparison of binding profiles between promoters and neuronal activity-regulated enhancers. a, b, Binding profiles of methylated histones and transcription factors at the promoter transcription start sites (TSSs) of 25,562 annotated genes (**a**) versus 5,117 extragenic enhancers (**b**). In each panel, binding profiles of methylated histones (top), CBP and NPAS4 (middle), and CREB and SRF (bottom) from unstimulated and membrane-depolarized (2 h KCl) neurons are shown. The *y* axes denote the degree of binding averaged across all promoters or enhancers, expressed as the mean number of input-normalized ChIP-Seq reads. Promoters are aligned at their annotated TSSs and enhancers are aligned at their CBP binding sites, with the *x* axes indicating the distance (kb) to either the TSS or the CBP peak.

surrounding CBP binding sites as enhancer domains (Fig. 2b, top, and Supplementary Fig. 1c). The enhancer domains have very low levels of H3K4me3 and are devoid of H3K27me3, a histone marker that has been shown to be associated with either repressed or inactive genes (Fig. 2b, top). Furthermore, the levels of these histone marks are not significantly changed with membrane depolarization, suggesting that enhancer domains are maintained in an open chromatin conformation that is accessible for transcription factor binding, even in the absence of gene induction.

We asked whether transcription factors that are known to mediate activity-regulated gene expression bind to enhancers constitutively or in an activity-regulated manner. CREB, SRF and NPAS4 are known activity-regulated transcription factors that have an important role in various aspects of brain development including neuronal survival, synapse development and synaptic plasticity[15,16]. We find in neurons that CREB, SRF and NPAS4 bind to neuronal enhancers as well as promoters (Supplementary Table 3). Although both CREB and SRF bind enhancers before membrane depolarization, their binding at enhancers in some cases seems to be increased upon membrane depolarization (Fig. 2, bottom, and Supplementary Figs 1d, 2, 4a and 5). In contrast, the binding of NPAS4, which is not present in neurons at significant levels before membrane depolarization[16], was not detected before stimulation but was found at ~28,000
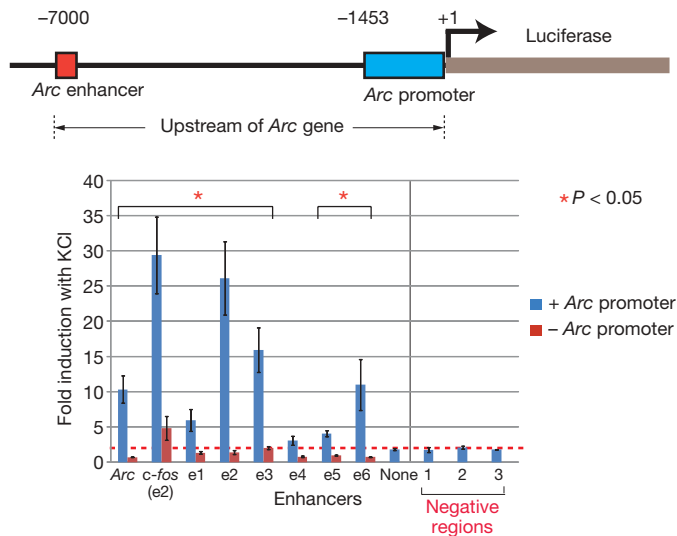
Figure 3 | Activity-induced luciferase expression mediated by neuronal enhancers. The *Arc* enhancer was replaced by six randomly chosen neuronal enhancers and one of the c-*fos* enhancers (e2; see Fig. 1) in the context of the ~7-kb region upstream of the *Arc* gene. The resulting fragments were placed upstream of a luciferase reporter gene, and activity-dependent expression of luciferase was measured in the presence or absence of the *Arc* proximal promoter after 6 h KCl treatment in rat cortical neurons. In additional control experiments, the *Arc* enhancer was removed, or three randomly chosen extragenic loci that do not show enhancer features were inserted. The red dotted line indicates the mean induction value of the three negative regions tested. Error bars indicate s.e.m. ($n = 3$ biological replicates); *P*-value from *t*-test.

sites in membrane-depolarized neurons (Figs 1, 2, middle, and Supplementary Figs 1e, 2 and 3). NPAS4 binding was strongly biased towards enhancers relative to promoters, suggesting that NPAS4 may have a specific role in enhancer function (Supplementary Fig. 4a). Although we have shown that enhancer domains can be as long as 4 kb, our analysis of CREB, SRF, NPAS4 and CBP binding to enhancers indicates that these factors are predominantly located within 100 bp of the highly conserved centre of the enhancer domain (Supplementary Fig. 4b). This tight co-localization of individual transcription factors with CBP at a subset of enhancers (Supplementary Table 4) suggests that transcription factors may work together to regulate enhancer function, possibly by recruiting CBP.

Transcription at enhancers

At promoters, CBP recruits components of the basal transcription machinery, including RNAPII, thereby facilitating the assembly of functional transcription complexes that initiate mRNA synthesis[17]. Because CBP binds to enhancers in an activity-dependent manner, we asked if CBP also recruits RNAPII to these enhancers. To address this issue, we used ChIP-Seq to identify RNAPII binding sites across the genome using two different RNAPII antibodies. Consistent with previous studies[18,19], a large number of RNAPII sites were found to be located near annotated TSSs (Figs 1, 4a and Supplementary Fig. 4a). Notably, RNAPII also bound to ~3,000 activity-regulated enhancers (25%) (Figs 1, 4b and Supplementary Figs 1f, 3 and 4a), and the level of RNAPII binding was increased about twofold upon membrane depolarization (Fig. 4b and Supplementary Fig. 2). Although RNAPII has previously been reported to be present at several enhancers, including the β-globin and MHC class II gene enhancers[20,21], it has not been thought to have a widespread role in enhancer function. Given that CBP was previously known to recruit RNAPII to promoters and that increases in CBP and RNAPII binding coincide at thousands of enhancers in membrane depolarized neurons, it is likely that CBP has a role in the activity-regulated increase in RNAPII binding at enhancers. However, the observation that RNAPII is present at only a
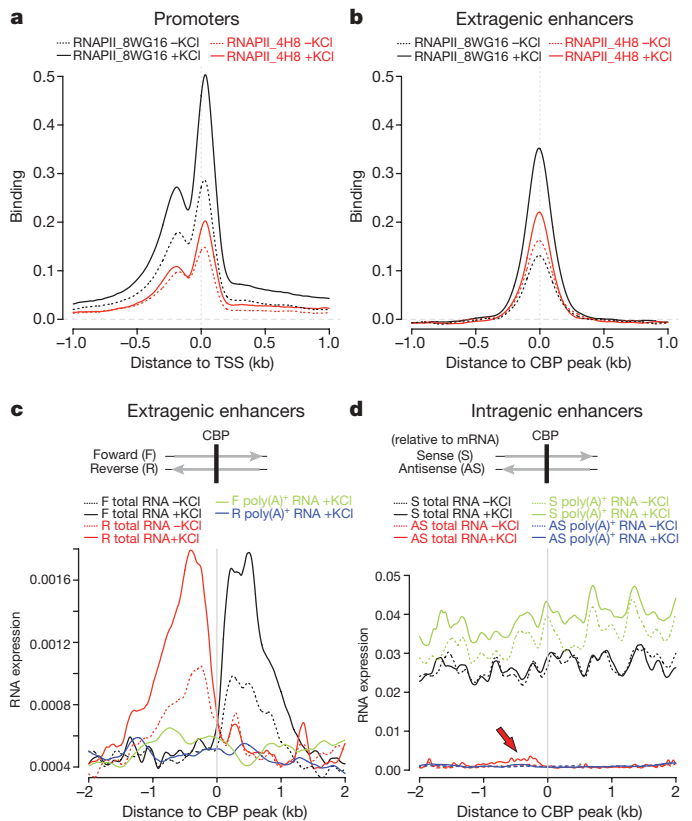

Figure 4 | Enhancers bind RNA polymerase II (RNAPII) and produce eRNAs. **a**, Binding profile of RNAPII at 25,562 TSSs of annotated genes using two different anti-RNAPII antibodies (8WG16 or 4H8). **b**, Binding profile of RNAPII at 5,117 extragenic enhancers. **c, d**, Profile of RNA expression at 5,117 extragenic enhancers (**c**) and at 6,718 intragenic enhancers (**d**) based on RNA sequencing of the total RNA and poly(A)$^+$ RNA fractions. The *y* axes report RNA expression as the normalized number of RNA-Seq reads per bp (Methods). In **c**, F and R denote forward (+) and reverse (−) genomic strands. In **d**, enhancers are aligned oriented relative to the gene in which they reside to allow for sense and antisense RNA-Seq reads to be shown separately. Although sense eRNAs cannot be detected due to overlapping mRNA transcription, the red arrow indicates a local increase in antisense RNA expression attributable to eRNAs (statistics in Methods). Note different scales on the *y* axis in **c** and **d**.

subset of CBP-bound enhancers suggests that additional activation steps beyond CBP binding may be required for RNAPII recruitment to enhancers.

The presence of RNAPII at enhancers raises the possibility that RNA transcription may occur at enhancers. Alternatively, the detection of RNAPII at enhancers might be an indirect consequence of the interaction of enhancers with active promoters, such that promoter-bound RNAPII gets crosslinked to enhancer DNA during the preparation of cells for ChIP-Seq experiments. To distinguish between these two possibilities, we used high-throughput RNA sequencing (RNA-Seq) to determine whether enhancer-bound RNAPII drives RNA synthesis at enhancers. Because it was not clear whether enhancer-derived transcripts would be polyadenylated, we sequenced total RNA, obtained from unstimulated or membrane-depolarized neurons after ribosomal RNA was depleted. To distinguish possible enhancer-derived transcripts from mRNA transcripts, we sought evidence of RNA transcription specifically at those ~5,000 activity-regulated enhancers located outside of annotated genes (extragenic enhancers). Surprisingly, we detected short (<2 kb) RNAs at ~2,000 extragenic enhancers (Figs 1, 4c, 5a, c and 6a). We observed dynamic changes in the levels of these enhancer RNAs (eRNAs) upon membrane depolarization, with a mean increase of ~2-fold (Fig. 4c). Synthesis of eRNAs seems to initiate near enhancer centres where CBP and RNAPII are bound and to proceed bi-directionally, extending to the
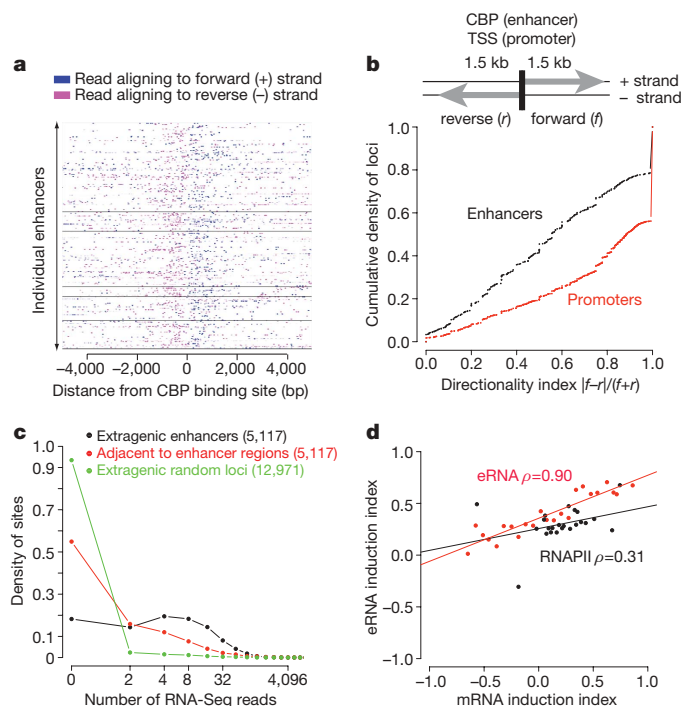
Figure 5 | eRNAs are transcribed bi-directionally, and their activity-dependent induction correlates with induction of nearby genes. a, RNA expression at 315 representative extragenic enhancers (see Methods for the enhancer selection and clustering). The enhancers are grouped into six categories using *k*-means clustering based on eRNA, RNAPII, CBP, NPAS4, CREB, SRF and H3K4me1 levels, with categories separated by horizontal black lines[3]. **b**, Directional bias of transcription initiated from enhancers and promoters, where *f* and *r* represent the numbers of reads (forward and reverse, respectively) aligning to the regions indicated (see Methods). **c**, The distribution of the number of RNA-Seq reads found within 1.5 kb of the extragenic enhancer loci, adjacent regions and random regions (see Methods). **d**, Changes in RNAPII binding and eRNA levels at extragenic enhancers versus changes in mRNA expression levels of nearby genes upon membrane depolarization. Each dot represents a set of genes that have similar mRNA induction indices and a corresponding set of enhancers nearby those genes (see Methods). The lines are the best linear fits to the points, and ρ is the Spearman correlation coefficient.

ends of the H3K4me1-modified enhancer domain (Figs 1, 4c, 5a, b, 6a and Supplementary Fig. 7a, b). Interestingly, we also detected eRNAs at ~1,000 of ~7,000 intragenic enhancers (Methods). Although high levels of mRNA transcription across intragenic enhancers prevented accurate quantification of eRNAs in the sense orientation, antisense eRNAs at intragenic enhancers were detectable and were similar in level to eRNAs at extragenic enhancers (Fig. 4c, d and Methods). These observations indicate that enhancers are not only sites where transcription factors bind and recruit RNAPII that might subsequently be delivered to promoters, but that enhancers are also sites where RNA synthesis occurs.

The strand-specific synthesis of eRNAs (Fig. 5a) and the dynamic changes in the level of eRNAs in response to neuronal activity suggest that the detection of eRNAs is not due to the sequencing of residual genomic DNA that is present in our purified RNA samples. Nevertheless, to confirm the existence of activity-regulated eRNAs at enhancers, we used an alternative method (DNaseI treatment followed by quantitative polymerase chain reaction with reverse transcription (RT–qPCR)) to detect these RNA transcripts (Supplementary Fig. 6). By RT–qPCR, we detected eRNAs at each of 18 enhancer loci tested. This result provides independent confirmation that the thousands of distinct eRNAs detected by RNA-Seq are bona fide RNA transcripts that are induced in an activity-dependent manner from neuronal enhancers.

We did not detect eRNAs in RNA-Seq from poly(A)$^{+}$ RNA fractions, suggesting that a large number of eRNAs may not be polyadenylated.

Although it is possible that some polyadenylated eRNAs are present but not detectable at our current sequencing depth, two independent lines of evidence suggest that a large number of eRNAs may not be poly-adenylated. First, using RT–qPCR, we observed that eRNAs were detected at higher levels in randomly primed reactions compared to oligo-dT-primed RT reactions (data not shown). Second, conventional sequencing of a circularized eRNA from the *Arc* enhancer confirmed that this transcript is not polyadenylated (Fig. 6). These experiments suggest that polyadenylation may not be a common feature of eRNA synthesis.

The detection of RNAPII binding and RNA synthesis at many enhancers could, in principle, result from mis-categorization of un-annotated promoters as enhancers. However, several lines of evidence suggest that both the extragenic and intragenic enhancers we have identified are indeed enhancers and are not un-annotated promoters. First, histone modification profiles at enhancers and annotated promoters are clearly distinguishable (Fig. 2, top, and Supplementary Figs 1c and 8a). Activity-regulated enhancers have high H3K4me1 and relatively low H3K4me3 levels, whereas promoters have lower H3K4me1 and high H3K4me3 levels. Second, the observation that eRNAs do not extend beyond the ~4-kb enhancer domain suggests that the eRNAs are much shorter (<2 kb for each strand) than transcripts initiated at most gene promoters (Figs 4c and 5a). Third, unlike promoters, enhancers do not produce detectable levels of polyadenylated RNA (Fig. 4c, d). Fourth, a promoter prediction algorithm (ProSOM)[22] revealed that fewer than 100 of ~12,000 enhancer regions are predicted to be promoters compared to 8,494 out of 27,854 annotated TSSs. Fifth, whereas sense transcription is more prevalent than antisense transcription at most promoters, transcription at enhancers seems to be less biased towards one particular strand (Fig. 5b). Finally, a few enhancers, including the well-characterized β-globin enhancer, have previously been shown to recruit RNAPII and drive transcription[23,24]. These findings argue against the possibility that RNAPII-bound enhancers that produce eRNAs are actually un-annotated promoters.

Mechanism of eRNA synthesis

Our observation that only a subset of the ~12,000 enhancers that inducibly bind CBP also bind RNAPII and drive eRNA transcription led us to hypothesize that RNAPII and/or eRNA synthesis might occur at a subset of enhancers that are actively engaged in promoting mRNA synthesis. To test this hypothesis, we investigated whether activity-regulated changes in RNAPII or eRNA levels at enhancers correlate with changes in mRNA levels at nearby genes (Fig. 5d and Supplementary Fig. 7c). The assumption in this analysis is that an enhancer is most likely to promote mRNA synthesis of the nearest gene[3,25]. We found that changes in eRNA expression levels that occur at enhancers upon membrane depolarization are strongly correlated with changes in mRNA expression levels at nearby genes. Changes in RNAPII levels at enhancers are also, to a lesser degree, correlated with changes in mRNA expression levels at nearby genes (Fig. 5d). Given that only a fraction of enhancers show inducible RNAPII binding or inducible eRNA synthesis, the binding of CBP to enhancers may not be sufficient for enhancer activation. Instead, enhancers exhibiting RNAPII binding and eRNA synthesis may represent a subset of CBP-bound enhancers that are actively engaged in promoting mRNA transcription.

The correlation between eRNA and mRNA induction suggests that eRNA synthesis may only occur when an enhancer interacts with the promoter of its target gene. In this scenario, eRNAs should not be generated from an enhancer when its target promoter is absent. We tested this hypothesis in the specific case of the mouse *Arc* enhancer using *Arc* knockout neurons in which most of the *Arc* gene, including the *Arc* promoter, is deleted but the *Arc* enhancer remains intact[10]. To characterize the *Arc* enhancer in *Arc* knockout neurons, we first performed chromatin immunoprecipitation (ChIP) experiments testing for the binding of SRF and RNAPII, two factors that we found
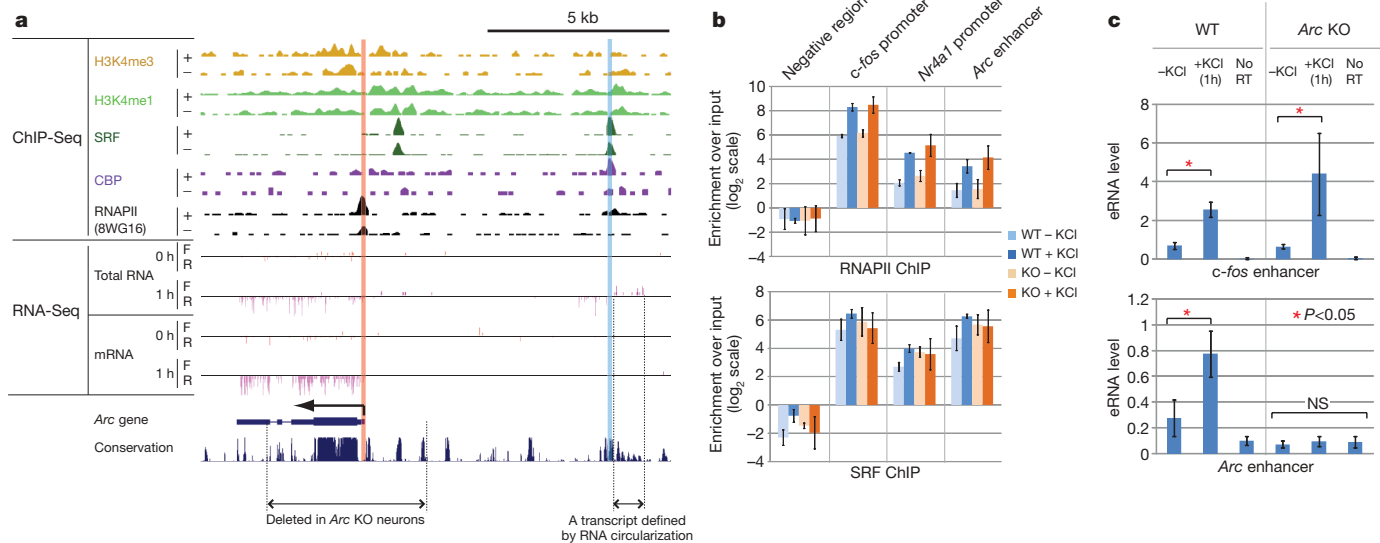
Figure 6 | eRNA synthesis but not RNAPII binding at the *Arc* enhancer requires the presence of the *Arc* promoter. a, The mouse *Arc* genomic locus with ChIP-Seq and RNA-Seq data as in Fig. 1. Also shown are the region deleted in the *Arc* knockout (*Arc* KO) mouse and a non-polyadenylated eRNA transcript defined by the RNA circularization method (Methods). **b**, Binding profiles of RNAPII and SRF at various loci determined by ChIP-Seq to be bound to the *Arc* enhancer (Fig. 6a, b)[13,14]. In *Arc* knockout neurons, both SRF and RNAPII remained bound at the *Arc* enhancer at levels equivalent to those observed in wild-type neurons, indicating that the binding of SRF and RNAPII to the *Arc* enhancer is independent of the *Arc* promoter. However, in the absence of the *Arc* promoter, we were not able to detect eRNA synthesis at the *Arc* enhancer (Fig. 6c). This absence of eRNA was specific to the *Arc* enhancer, as we observed robust induction of eRNA at a c-*fos* enhancer in the *Arc* knockout neurons. These results demonstrate that the recruitment of RNAPII to the *Arc* enhancer is not sufficient to drive eRNA synthesis and suggest that, like mRNA synthesis, eRNA synthesis may require an interaction of the enhancer with a promoter.

Discussion

We provide genome-wide evidence that thousands of neuronal activity-regulated enhancers that are defined by activity-independent H3K4me1 marks and activity-dependent CBP binding also recruit RNAPII and produce eRNAs. The observation of widespread RNAPII binding at enhancers suggests that a general mechanism of activity-dependent enhancer function in neurons may involve recruitment of RNAPII to enhancer loci, followed by subsequent transfer of RNAPII to promoters. Previous studies of a few individual enhancer loci have proposed several models for delivery of RNAPII from an enhancer to a promoter, including tracking of RNAPII along DNA and direct transfer of RNAPII via DNA looping[20]. Our observation that eRNAs are produced only within 2-kb enhancer domains and not along the entire distance between enhancers and promoters indicates that transcription-dependent RNAPII tracking is not likely to be a widespread mechanism of RNAPII delivery.

Our finding that large numbers of neuronal activity-regulated enhancers recruit RNAPII implies that enhancers may be more similar to promoters than previously appreciated. However, our analysis of the *Arc* enhancer in neurons lacking the *Arc* promoter demonstrates that the transcriptional machinery assembled at the *Arc* enhancer is not able to drive transcriptional initiation without the *Arc* promoter. This finding may explain why the level of eRNA synthesis is correlated with the level of transcription at the nearest promoter, and it suggests that eRNA synthesis at many enhancers may require a dynamic interaction between an enhancer and a promoter.
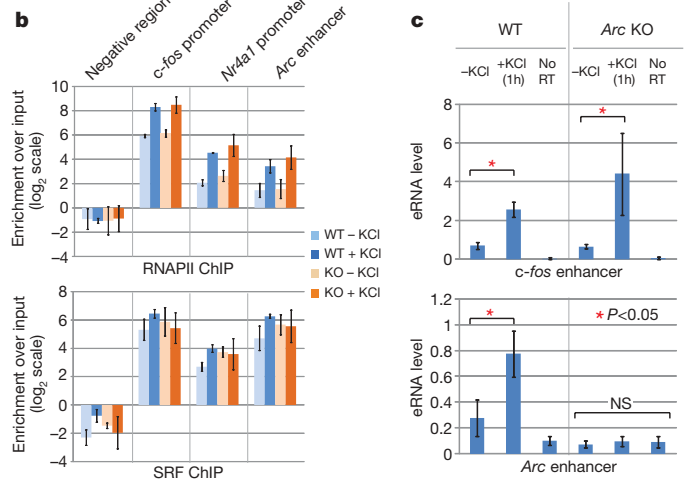
ChIP-qPCR from both wild-type and *Arc* knockout neurons. Error bars indicate s.e.m. ($n = 2$ biological replicates) **c**, RT–qPCR detection of the presence of eRNAs from wild-type and *Arc* knockout neurons. 'No RT' represents the qPCR signal from cDNA samples generated from reactions in which reverse transcriptase was omitted. Error bars are s.e.m. ($n = 3$ biological replicates); *P*-values are from *t*-test. NS, not significant.

A remaining question is whether eRNAs have a specific biological function. In one model, the RNAPII-dependent transcriptional process at enhancers itself, rather than the eRNA transcripts it produces, may be important for enhancer function. For example, RNAPII has previously been shown to recruit chromatin-modifying enzymes such as histone methyltransferases[26]. In this regard, it is noteworthy that eRNAs are observed only within the H3K4me1-modified enhancer domain, and the level of the H3K4me1 modification and the level of eRNA synthesis are tightly correlated (compare Figs 2b, top, and 4c). Thus, the process of eRNA synthesis could be required to establish and maintain a chromatin landscape at enhancers that is required for enhancer function. However, it is also possible that the eRNA transcripts themselves are functionally important. The ability of enhancers to be transcribed in a regulated manner may provide an evolutionary mechanism by which new, functionally important genes or non-coding RNAs are generated.

METHODS SUMMARY

Directionality index at promoters and enhancers. A directionality index was defined as $|f - r|/(f + r)$, where f is the number of divergent reads on the forward strand and r is the number of divergent reads on the reverse strand within 1.5 kb of the CBP peak or TSS. (See Fig. 5b.)

Calculating the number of extragenic enhancers that produce eRNAs. The level of eRNA for each enhancer locus is calculated by counting all RNA-Seq reads found within a 1.5-kb region on both sides of the CBP peak. As a control, we consider the number of reads found in the adjacent regions (-3.5 kb to -2 kb) and ($+2$ kb to $+3.5$ kb) relative to the CBP peak, and in random regions. If one requires >7 reads for detection, 2,267 or 44% of the enhancers have eRNAs, compared to 16% of the flanking regions and 2% of the random regions. (See Fig. 5c.)

Changes in eRNA levels and RNAPII binding at enhancers. For changes in RNAPII binding at enhancers, we counted the number of ChIP-Seq reads within 300 bp of the enhancer centre at each time point. For eRNAs, we used the same procedure, including all reads within 1.5 kb of the enhancer. We defined the normalized induction index as $(s - u)/(s + u)$, where s and u are the number of normalized reads from the stimulated and unstimulated conditions, respectively. (See Fig. 5d.)

Correlations between enhancer features and mRNA expression levels at nearby genes. We paired each enhancer with the nearest TSS, provided that the distance was <1 Mb. The induction index for RefSeq genes was calculated as before for RNAPII, but based on the average read density throughout the coding region for mRNA. Genes were grouped by induction ratio quantiles into 25 bins before plotting. (See Fig. 5d.)

1. Banerji, J., Rusconi, S. & Schaffner, W. Expression of a β-globin gene is enhanced by remote SV40 DNA sequences. *Cell* **27**, 299–308 (1981).
2. Greer, P. L. & Greenberg, M. E. From synapse to nucleus: calcium-dependent gene transcription in the control of synapse development and function. *Neuron* **59**, 846–860 (2008).
3. Heintzman, N. D. *et al.* Distinct and predictive chromatin signatures of transcriptional promoters and enhancers in the human genome. *Nature Genet.* **39**, 311–318 (2007).
4. Visel, A. *et al.* ChIP-seq accurately predicts tissue-specific activity of enhancers. *Nature* **457**, 854–858 (2009).
5. Xi, H. *et al.* Identification and characterization of cell type-specific and ubiquitous chromatin regulatory structures in the human genome. *PLoS Genet.* **3**, e136 (2007).
6. Park, P. J. ChIP-seq: advantages and challenges of a maturing technology. *Nature Rev. Genet.* **10**, 669–680 (2009).
7. Barski, A. *et al.* High-resolution profiling of histone methylations in the human genome. *Cell* **129**, 823–837 (2007).
8. Robertson, A. G. *et al.* Genome-wide relationship between histone H3 lysine 4 mono- and tri-methylation and transcription factor binding. *Genome Res.* **18**, 1906–1917 (2008).
9. Chowdhury, S. *et al.* Arc/Arg3.1 interacts with the endocytic machinery to regulate AMPA receptor trafficking. *Neuron* **52**, 445–459 (2006).
10. Plath, N. *et al.* Arc/Arg3.1 is essential for the consolidation of synaptic plasticity and memories. *Neuron* **52**, 437–444 (2006).
11. Shepherd, J. D. *et al.* Arc/Arg3.1 mediates homeostatic synaptic scaling of AMPA receptors. *Neuron* **52**, 475–484 (2006).
12. Waltereit, R. *et al.* Arg3.1/Arc mRNA induction by Ca^{2+} and cAMP requires protein kinase A and mitogen-activated protein kinase/extracellular regulated kinase activation. *J. Neurosci.* **21**, 5484–5493 (2001).
13. Kawashima, T. *et al.* Synaptic activity-responsive element in the Arc/Arg3.1 promoter essential for synapse-to-nucleus signaling in activated neurons. *Proc. Natl Acad. Sci. USA* **106**, 316–321 (2009).
14. Pintchovski, S. A., Peebles, C. L., Kim, H. J., Verdin, E. & Finkbeiner, S. The serum response factor and a putative novel transcription factor regulate expression of the immediate-early gene Arc/Arg3.1 in neurons. *J. Neurosci.* **29**, 1525–1537 (2009).
15. Flavell, S. W. & Greenberg, M. E. Signaling mechanisms linking neuronal activity to gene expression and plasticity of the nervous system. *Annu. Rev. Neurosci.* **31**, 563–590 (2008).
16. Lin, Y. *et al.* Activity-dependent regulation of inhibitory synapse development by Npas4. *Nature* **455**, 1198–1204 (2008).
17. Kee, B. L., Arias, J. & Montminy, M. R. Adaptor-mediated recruitment of RNA polymerase II to a signal-dependent activator. *J. Biol. Chem.* **271**, 2373–2375 (1996).
18. Brodsky, A. S. *et al.* Genomic mapping of RNA polymerase II reveals sites of co-transcriptional regulation in human cells. *Genome Biol.* **6**, R64 (2005).
19. Kim, T. H. *et al.* A high-resolution map of active promoters in the human genome. *Nature* **436**, 876–880 (2005).
20. Koch, F., Jourquin, F., Ferrier, P. & Andrau, J. C. Genome-wide RNA polymerase II: not genes only! *Trends Biochem. Sci.* **33**, 265–273 (2008).
21. Szutorisz, H., Dillon, N. & Tora, L. The role of enhancers as centres for general transcription factor recruitment. *Trends Biochem. Sci.* **30**, 593–599 (2005).
22. Abeel, T., Saeys, Y., Rouze, P. & Van de Peer, Y. ProSOM: core promoter prediction based on unsupervised clustering of DNA physical profiles. *Bioinformatics* **24**, i24–i31 (2008).
23. Ling, J. *et al.* HS2 enhancer function is blocked by a transcriptional terminator inserted between the enhancer and the promoter. *J. Biol. Chem.* **279**, 51704–51713 (2004).
24. Zhao, H. & Dean, A. An insulator blocks spreading of histone acetylation and interferes with RNA polymerase II transfer between an enhancer and gene. *Nucleic Acids Res.* **32**, 4903–4919 (2004).
25. Heintzman, N. D. *et al.* Histone modifications at human enhancers reflect global cell-type-specific gene expression. *Nature* **459**, 108–112 (2009).
26. Gerber, M. & Shilatifard, A. Transcriptional elongation by RNA polymerase II and histone methylation. *J. Biol. Chem.* **278**, 26303–26306 (2003).

Author Contributions T-K.K., J.M.G. and M.E.G. conceived and designed experiments. T-K.K., J.M.G., M.H., G.K. and M.E.G. wrote the manuscript. T-K.K. optimized the protocol for ChIP-Seq library preparation to be suitable for the SOLiD sequencer and made all ChIP-Seq libraries used in this study. S.K. invented the library construction methodology used for all RNA sequencing reported here. J.M.G., A.M.C. and E.M.-P. made all RNA-Seq libraries. M.H., J.M.G. and D.A.H. performed bioinformatic analyses. K.B.-H. carried out the SOLiD bead preparation and sequencing. T-K.K., J.W., P.F.W. and A.M.C. performed the *Arc* knockout experiment. D.M.B. performed the luciferase experiments. M.L. performed the RNA circularization experiment. H.B. provided the pArc7000 plasmid. D.K. provided the *Arc* knockout mouse. All authors reviewed the manuscript.

Author Information Sequencing data have been submitted to the GEO repository under accession numbers GSE21161 (for all ChIP-Seq and RNA-Seq data) and HM047267 (for circularized *Arc* enhancer RNA). The bigWig files for genome browser visualization are posted online (see Supplementary Table 6). Reprints and permissions information is available at www.nature.com/reprints. The authors declare no competing financial interests. Correspondence and requests for materials should be addressed to M.E.G. (michael_greenberg@hms.harvard.edu).

METHODS

Mouse cortical cultures. E16.5 C57BL/6 mouse embryo cortices were dissected and then dissociated in $1\times$ Hank's Balanced Salt Solution (HBSS), 20 mg ml^{-1} trypsin (Worthington Biochemicals), and 0.32 mg ml^{-1} L-cysteine (Sigma) for 10 min. Trypsin treatment was terminated with three 2-min washes in $1\times$ HBSS with 10 mg ml^{-1} trypsin inhibitor (Sigma). Trituration of cells was performed with a flame-narrowed Pasteur pipette to dissociate cells fully. Neurons were seeded at an approximate density of 4×10^7 on 15-cm dishes. The dishes were pre-coated overnight with poly-ornithine (30 µg ml^{-1}, Sigma) in water, washed three times with water, and washed once with Neurobasal Medium (Life Technologies) before use. Neurons were maintained in 30 ml Neurobasal Medium containing B27 supplement (2%; Invitrogen), penicillin-streptomycin (50 µg ml^{-1} penicillin, 50 U ml^{-1} streptomycin, Sigma) and glutamine (1 mM, Sigma). Neurons were grown *in vitro* for 7 days. Eight millilitres of the medium was replaced with 10 ml fresh warm medium on the 4th and 6th days *in vitro*.

Membrane depolarization by applying extracellular potassium chloride (KCl). For KCl depolarization of neurons, days *in vitro* (DIV) 6 neurons were quieted overnight in 1 µM tetrodotoxin (TTX, Tocris) and 100 µM D(-)-2-amino-5-phosphonopentanoic acid (D-AP5, Tocris), and they were incubated for 0, 1, 2, or 6 h in 55 mM KCl. ChIP-Seq experiments made use of 0 or 2 h KCl treatment. RNA-Seq experiments were performed with 0, 1, or 6 h of KCl treatment. Luciferase assays were done at 6 h KCl.

Luciferase reporter assays. For testing enhancer functionality, we randomly selected seven extragenic enhancers and tested their ability to function as activity-regulated enhancers in a transfection assay in cultured rat cortical neurons. We transfected DIV 5 neurons using the calcium phosphate method. As a positive control, we used the pGL4.11-Arc7000-luc2P plasmid[27], hereafter referred to as pArc7000, consisting of 7 kb of sequence upstream of the *Arc* coding region. As a negative control, we used pGL4.11-Arc7000-del no 1.luc2P, hereafter referred to as pArc7000-del1, which lacks a 5' ~250-bp fragment corresponding to the synaptic activity response element (SARE)[27] located 7 kb upstream of the *Arc* gene. To test candidate enhancers, we replaced the SARE (XhoI-SwaI) with ~1-kb fragments centred on the CBP peaks at candidate enhancers. For the negative control loci, we choose three genomic regions where we observed no factor binding (ChIP-Seq) and no RNA expression (RNA-Seq). To excise the *Arc* proximal promoter from each of the candidate enhancer plasmids, we cut with HindIII and re-circularized, which removes two HindIII fragments totalling 1.4 kb.

qPCR validation of eRNA expression and activity induction. For validating eRNA expression, we chose 18 eRNA transcripts that were detected within 1.5 kb of the CBP site. We isolated RNA from three biological replicate KCl experiments at 0, 1 and 6 h of KCl using Trizol (Invitrogen). Each RNA sample was treated with DNaseI (Invitrogen, amplification-grade DNaseI). After the treatment each RNA sample was brought to a volume of 300 µl by the addition of Nuclease Free Water (Ambion), and precipitated with Glycogen (Ambion 5 mg ml^{-1},1:100), 3 M NaOAc (Ambion, 1:10) and 2.5 volumes of 100% ethanol. Reverse transcription of the precipitated RNA was performed using the High Capacity cDNA synthesis kit (Applied Biosystems) with random priming. The cDNA was the source of input for quantitative PCR, using a Step One Plus Real-Time PCR Instrument and SYBR Green reagents (Applied Biosystems). Each primer set used in the analysis was validated using a standard curve obtained from serial dilutions of genomic DNA. Each primer set included in the analysis had melt curves that were consistent with the amplification of a single product in the expected size range. The detectability plot was constructed with concentration values normalized to genomic DNA in the case of eRNA primers, or dilutions of cDNA for gene primers. The inducibility plot was constructed using concentration values that were normalized to corresponding tubulin concentrations.

RNA isolation. RNA was isolated from cultures using 30 ml Trizol on each 15-cm culture dish according to the manufacturer's instructions (Life Technologies). Up to four dishes were solubilized using the same 30 ml Trizol for a yield of 500–1,000 µg total RNA.

To define the 5' and 3' termini of uncharacterized RNAs, we circularized RNA, reverse-transcribed circular RNAs using random priming, and PCR-amplified the ligation junctions for conventional sequencing. We generally followed the protocol from ref. 28 with exceptions noted below.

(1) Total RNA from 1-h KCl-treated neurons was first treated with DNaseI as follows: 100 µg of RNA was incubated with 100 units of DNaseI, Amplication Grade (Invitrogen) in 1 ml of the supplied $1\times$ buffer. Then 100 µl of 25 mM EDTA was added and the DNaseI was deactivated at 75 °C for 10 min. RNA was extracted with phenol and chloroform and precipitated with ethanol.

(2) Next we decapped the DNaseI-treated RNA as follows: 10 µg of the RNA was incubated with 25 units of tobacco acid pyrophosphatase (that is, TAP) (Epicentre) in the provided $1\times$ buffer at 37 °C for 1 h. RNA was extracted with phenol and chloroform and precipitated with ethanol.

(3) RNA was circularized using T4 DNA ligase as follows: 8 µg of RNA in 2 ml of 50 mM Tris-HCl (pH 7.6), 10 mM MgCl$_2$, 1 mM ATP, 5% PEG-8000 was incubated with 20 units of T4 RNA ligase (Invitrogen) for 18 h at 37 °C. The ligase was inactivated at 65 °C for 10 min. RNA was extracted with phenol and chloroform and precipitated with ethanol.

(4) Reverse transcription was performed as described with the following modifications: we synthesized cDNA using 1 µg of circularized RNA as a template for cDNA synthesis and random hexameric primers following the Superscipt III reverse transcriptase kit (Invitrogen) in 20 µl reactions.

(5) PCR amplification was performed using a nested PCR approach. Primers were designed to amplify across possible 5'–3' junctions. First, primary reactions were as follows: 1 µl of cDNA was cycled with 1 µM of each primary primer (Arc_R2new: AGGGTACAAGTAAACAAATACCTGA and Arc_L9new: AGT TCTCTAGCTAAGGCAAGCA) in Power SYBR (Applied Biosystems) mix in a total of 20 µl. Reactions were cycled as follows: 95 °C for 10 min and 20 cycles of 95 °C for 15 s, 60 °C for 30 s and 72 °C for 3 min. Second, the primary PCR reaction was further amplified on a qPCR machine using nested primers as follows: 10 µl of the primary PCR was cycled with 1 µM of each nested primer (Arc_R1new: TTAAGAGTCACAAAGCCACCAAT, Arc_L10new: GTCTCTAC CATTGATGGATCTC) in a 2 ml Power SYBR reaction divided into multiple wells. Nested PCR was performed as follows: 95 °C for 10 min and 40 cycles of 95 °C for 15 s, 60 °C for 1 min. Product was purified using QIAQuick PCR purification columns and sequenced conventionally. The product was mapped to the eRNA region using the UCSC Genome Browser (BLAT).

The sequence of the transcript obtained from this method is: ArcE1 + strand transcript, GGAGAGGTGGGGACCAGAGTCCCTGGCTGGAGACTGGTGAC ATTGTCCCTGCCATTGGTGGCTTTGTGACTCTTAAACCAGACCTGCACA AAGATCTTGTATCAGGTATTTGTTTACTTGTACCCTAGAGCTCTGGTTC CAGGAGAAAGCAGATGGCCCCCCGGGTGGGGGGGCCCTGGGCAGTAG TAGCTCCTCAGTCCTGTAAATAAATCCCTAGGAACAGCGTTCAGGCTG AAGGGTTCGAGCTCTGGGCTGGGCGTACACCAGCGCCAAGATGCAGA CAGGTAAGAATGCTTAGAATTCCTGTGCCTGACATTTCTCATTCTGTCA CAAAGGGGAGTGGGGTACCAATAGGGATGGAGCACAGTGCCCTGAAA GAGTTCAGATTCACACAGAGAACCAGGAAGGGCTTCCTAGAGGTGGAG CCTGTGGGTAGAAGGCAAAGAGCACAGGTTGAGCAGGGGAGGCCAGT GCTGTGTCCCCTCCACTCTTTTGGCTCCCTAATGGCCTTCAAGCGTGG TTACCCTCCTCTGGCTGGTGACTCCTCCGTTTTCTCTCTGGGCGGGGA GGGTGTTGGATCTGGACCTCTTTCTTTCTCCGATGTCTCCTCCTACCAG AGGCAGCTCATCTGAGTTCTCAAGCCTTTGCCCTGGGCTTTGAAACTG ACAACCAGCTCCCAGTGAGTGACCTGTGGAGCTGCAGACATGTGGAGA TCCAAGTTGTCTCCCCACTTCCTGTAGTTCTCTAGCTAAGGCAAGCAG GTCTCTACCATTGATGGATCTCACAGGTACCAGGCACGACTCTCGGTC CCTCGACCCACTGGAAAAGGTTGTGCATGGGTTCAGGGT.

SOLiD sequencing. SOLiD sequencing of ChIP-Seq and RNA-Seq libraries were performed on a SOLiD instrument (1, 2, or 3.0 version) with 35-bp reads according to manufacturer's instructions (Life Technologies). All experiments were performed on full sequencing slides with barcodes used to distinguish up to 16 sequencing libraries on a slide. Libraries were quantified by SYBR green quantitative-PCR (qPCR) to determine appropriate mixing ratios, which also depended on the desired sequencing depth for each of the libraries in the mixture.

Chromatin immunoprecipitation sequencing (ChIP-Seq). Forty million mouse cortical neurons cultured to *in vitro* day 7 were used for each ChIP-Seq library construction. ChIP was performed as described[29] using antibodies listed above. The immunoprecipitated DNA fragments were repaired by the End-It DNA End Repair Kit (Epicentre Biotechnology) according to the manufacturer's instructions. The end-repaired ChIP DNA fragments were purified by MinElute Reaction Cleanup Kit (Qiagen) and eluted in 20 µl in EB buffer. The resulting DNA fragments were ligated with P1 and P2 adaptors for SOLiD genome analyser (adaptor sequences can be made available upon request) for 20 min at room temperature using the Quick Ligase Kit (NEB), followed by purification using the MinElute Reaction Cleanup Kit (Qiagen). The purified, adaptor-ligated ChIP DNA fragments were subject to 6% native-PAGE for an in-gel PCR reaction. A gel slice containing 175–200 bp adaptor-ligated ChIP DNA fragments (corresponding to 125–150 bp genomic fragment sizes) was cut and shredded. PCR Platinum Supermix (100–200 µl, Invitrogen), 50 pmol of PCR primers (available upon request), 0.5 µl Taq DNA polymerase (NEB), and 0.15 µl p.f.u. Turbo DNA polymerase (Stratagene) were added into the shredded gel slice. The adaptor-ligated ChIP DNA fragments were amplified by 15 cycles of in-Gel PCR. After the PCR reaction, gel pieces were filtered out by 0.45 µm filter spin column, and the amplified ChIP-Seq library was purified by the MinElute PCR purification kit (Qiagen). The library was purified by one more round of 6% PAGE. A gel slice containing 200–250 bp PCR products (110–150 bp fragment size) was cut and shredded, and the amplified library was extract out of the gel by passive elution in elution buffer (1.5 M ammonium acetate in $1\times$ TE). Gel pieces were

filtered out by filter spin column, and the resulting ChIP-Seq library was purified using the Qiaquick PCR purification kit (Qiagen).

Whole-transcriptome sequencing (WT-Seq: sequencing of total RNA). WT-Seq was performed according to a protocol/kit now available from Life Technologies, with minor modifications that are included below. Briefly, 5–10 μg of RNA isolated from mouse cortical cultures was depleted of ribosomal RNAs using two rounds of Human/Mouse RiboMinus treatment (Life Technologies) with overnight ethanol precipitations for sample re-concentration. The removal of ribosomal RNAs was confirmed on a Bioanalyser Nano Chip (Agilent). A total of 500–1,000 ng of riboRNA-depleted total RNA was fragmented with 10–18 min at 37 °C RNaseIII treatment, and 10 min of RNaseIII inactivation at 65 °C. Fragmentation was followed by size selection of ~50 to ~150 bp fragments using the flashPAGE denaturing PAGE-fractionator (Life Technologies) and ethanol precipitation overnight. The resulting RNA was directionally ligated, reverse-transcribed and RNaseH treated.

After trial PCR to assess library quality and quantity, 30 μl cDNA was run on a native 6% PAGE gel. The 90–120-bp size window (corresponding to 50–80-bp RNA insert size) was cut from the gel, shredded and inserted directly into a 400 μl PCR reaction using standard WT-Seq kit components and submitted to 11–15 cycles of PCR. The PCR product was phenol-chloroform extracted, ethanol precipitated and re-suspended in 20 μl WT-Seq gel loading buffer. The resulting sample was run on a 6% native PAGE gel, and the 150–175-bp size range (corresponding to 60–85 bp) was cut from the gel, shredded, and extracted overnight in WT-Seq PAGE elution buffer. The resulting library was filtered through 0.45 μm spin filters (Life Technologies) to remove gel pieces and ethanol precipitated.

We note that WT-Seq can detect neither the 5′-most fragment from transcripts with 5′-modified ends (such as mRNA 5′ 7-methyl-guanosine caps) nor the 3′-most fragment from transcripts with 3′-modified ends. However, for transcripts long enough to produce multiple ≥50-bp fragments, WT-Seq should detect the remaining fragments.

Mouse cortical neuron WT-Seq data presented in this manuscript are from one specific biological replicate, but each result was confirmed in at least one additional replicate.

mRNA sequencing (mRNA-Seq). mRNA-Seq was performed exactly as WT-Seq, except that the ribosomal RNA-removal steps were replaced by two rounds of polyA purification using the FastTrack MAG mRNA isolation kit (Life Technologies). The removal of ribosomal RNAs was confirmed on a Bioanalyser Nano Chip (Agilent).

Annotation version and mRNA TSS collection. For filtering CBP peaks to remove TSSs, we used all TSSs from UCSC known genes, Ensembl genes and RefSeq genes. The NCBI reference sequence (RefSeq) collection of mouse gene annotation, version 37_1, was used for analysing TSSs for comparison with enhancers (for example, Fig. 2a). A subset of RefSeq genes has multiple annotated TSSs per gene, and we used for these analyses only the 5′-most TSSs from these genes. Thus, 25,562 TSSs were used instead of the full set of 27,854 RefSeq TSSs.

Read alignment (mapping sequencing reads to the genome and splice junctions). ChIP-Seq, WT-Seq and mRNA-Seq sequencing reads were aligned using the large genomes matching pipeline from Life Technologies with parameters –e 3 –t 35 –z 10. These parameters dictate that 0–3 colour-space mismatches are allowed, a 35-bp read is aligned, and after 10 hits on a given chromosome, the aligner no longer looks for further matches. ChIP-Seq reads were aligned to the mouse NCBI genome version 37. WT-Seq and mRNA-Seq reads were also aligned to mouse NCBI 37, but in their cases, the genome was expanded with addition of a pseudo-chromosome consisting of exon–exon splice junctions, although reads aligning to splice junctions were used solely to assess the strand specificity of WT-Seq (next section). Only reads aligning to a single genomic position with a tolerance of 0–3 colour-space mismatches were used for findings reported in this manuscript.

ChIP-Seq read-length extension. After ChIP-Seq reads were aligned, they were extended to 120 bp to match the length of the DNA fragments that were sequenced. We chose to extend to 120 bp based on experimental considerations (see ChIP-Seq procedure, above), but we also confirmed that this was a reasonable extension distance bioinformatically using the procedure introduced by ref. 30.

Peak finding from ChIP-Seq. Chromatin immunoprecipitation followed by high-throughput sequencing (ChIP-Seq) experiments produces a large number of short (~120 bp) DNA fragments which are enriched in the regions where the transcription factor of interest was bound to the DNA. The resulting profile of the mapped short sequence reads to the DNA shows which regions are enriched for the transcription factor in question. As an example of such a profile, consider Fig. 1. The next challenge is to determine which of the enriched regions ('peaks') are statistically significant at a given threshold and what regions correspond to genomic background. The background is given by sequencing the input genomic DNA fragments. Thus, a peak is defined as a region that contains significantly

more reads from the ChIP experiment than from the input control. We first determined the false discovery rate by using a sliding window with a width of 240 bp for every 10 bp in the mouse genome. Owing to repetitive sequences, it is impossible to assign 35-bp reads uniquely to some regions[31,32]. Consequently, such regions are excluded from our analysis. For each window, we calculated the statistic $D = R - N$ where R is the number of reads from ChIP, and N is the number of reads from an input sample. By considering the marginal distributions of R and N, we note that they both can be well approximated by a Poisson distribution with parameters λ_R and λ_N, respectively. It follows that D is a Skellam distribution[33]:

$$\Pr(D=d) \approx \text{Ske}(d; \lambda_R, \lambda_N) = e^{-(\lambda_R + \lambda_N)} \left(\frac{\lambda_R}{\lambda_N}\right)^{d/2} I_{|d|}\left(2\sqrt{\lambda_R \lambda_N}\right) \quad (1)$$

where $I_{|d|}(z)$ is the modified Bessel function of the first kind of order $|d|$. When comparing the number of reads in a given window from two different samples, care must be taken to correct for differences in the total amount of sequenced reads. The construction of the null distribution from equation (1) takes unequal numbers of reads in the two samples into account by shifting the mode of the distribution so that mode will be positive if there are more ChIP reads than input control reads and negative if there are more reads for the input control sample. To determine the number of reads required for a 240-bp window to be significant, we use the local false discovery rate (locFDR) framework[34]. Using this methodology, we assume that the density of D, $f(D)$, can be written as the mixture $f(D) = p_0 f_0(D) + p_1 f_1(D)$, where f_0 is the null density, f_1 is the density of windows corresponding to true peaks and $p_0 + p_1 = 1$ with $p_0 \geq 0.9$. The locFDR, FDR(d), is related to the more familiar FDR[35] through

$$\text{FDR}(d) = E[\text{locFDR}(d)|D \geq d] \quad (2)$$

where E is the expectation with respect to the mixture density f. Taking CBP as an example, with a fixed threshold $f_p = 0.01$ and empirically estimated $\lambda_R = 0.346$ and $\lambda_N = 0.419$, we find that the critical difference is $d_0 = 5$ fragments. Inserting the empirical distribution and the Skellam null distribution from equation (1), we find that the FDR is $\sim 3 \times 10^{-6}$. For the H3K4me1 peaks, the procedure described above was used, except that the window size was changed to 1,000 bp at increments of 100 bp. The motivation for using a larger window size is that histone modifications are typically much broader than transcription factor binding sites and using a larger window allows us to consider a signal from a larger genomic region and the process becomes less sensitive to noise. The parameters for the Skellam distribution were $\lambda_R = 11.88$ and $\lambda_N = 1.33$, and from equation (2) we estimate the FDR to be $\sim 2 \times 10^{-5}$.

Reproducibility. To verify that our findings are robust and reproducible, we sequenced at least one biological replicate of each ChIP-Seq and RNA-Seq experiment. The correlations of enrichment (ChIP-Seq) or read numbers (RNA-Seq) are high, except in cases (such as enhancers with few RNA-Seq reads) where sensitivity is poor. We present scatter plots of replicates in Supplementary Fig. 10. In the specific case of CBP, we had one ChIP-Seq experiment using the Millipore antibody and several others using an Abcam antibody. As is often the case in ChIP experiments, the quality of the two experiments varied, with the Millipore antibody performing much better in terms of the proportion of reads under peaks. The quality of the CBP peaks are important for subsequent analysis, both in terms of their number (higher numbers result in better statistical power in downstream analyses) and their quality (false positive CBP sites will reduce the apparent fractional number of enhancers with RNAPII binding and eRNA expression). Thus, we took extra care to select high-confidence CBP sites. First, we used our highest quality ChIP-Seq (using Millipore CBP antibody) to call 41,148 peaks. Of these, 4,567 were also called as peaks in several Abcam ChIP-Seq experiments. In addition, we found that the enrichment of reads from the Abcam ChIP-Seq at the remaining 36,601 loci was substantially above the levels seen at randomly chosen regions. Thus, to gain additional sensitivity in identifying replicated peaks, we set a 0.1 false discovery rate (FDR) based on the 90th percentile of CBP Abcam enrichment at random loci. 23,346 CBP Millipore peaks not called as peaks in the Abcam IP were nonetheless found to be above the 0.1 FDR (Supplementary Fig. 11a). Thus, our final set of validated CBP peaks is 4,567 + 23,457 = 28,024 (Supplementary Fig. 11b).

Alternative peak-finding method. Because the location of the CBP peaks is key to all further analyses for this paper, we validated the results using another peak-finding algorithm called Sissrs[36]. We assumed a fragment length of 120 bp and we used an FDR of 0.001, but other than that, the default settings were not changed. Sissrs reported 32,656 CBP peaks (CBP Millipore, 2 h KCl), and we found that 31,842 (97.5%) of those were located within 1 kb of the peaks detected using our method. Using a more stringent threshold of 100 bp, 83% of the Sissrs peaks were found near one of our peaks. For the unstimulated condition, Sissrs reported

8,980 peaks, significantly more than we found. Closer inspection reveals that all of our peaks were within 1 kb of a Sissrs peak and 78% were within 100 bp. All peaks discovered by both our method and Sissrs for the unstimulated condition show a high degree of induction (Supplementary Fig. 9), indicating that the degree of CBP binding before KCl stimulation is very low.

Normalization of ChIP-Seq and RNA-Seq read numbers. To compensate for differences in total sequencing read depth among samples, all ChIP-Seq read counts were first normalized to their equivalent numbers assuming 10 million total reads per sample. Next, the normalized number of reads in the IP was subtracted from the normalized number of reads in the input within a 240-bp scanning window, and the subtracted value was used for further analysis and plotting. We refer to these two procedures respectively as normalization and input-subtraction. A similar procedure was performed for RNA-Seq data, where read counts were normalized to their equivalent numbers assuming 50 million reads per sample, and the normalized values were used for further analysis and plotting. Because ChIP-Seq reads correspond to the ends of larger DNA fragments produced by sonication, we extended each ChIP-Seq read to 120 bp.

Selecting random control regions. To generate a set of random peaks matching the CBP peaks we did the following for each intragenic peak: (1) calculate the distance d to the TSS of the overlapping gene; (2) select a gene g at random; (3) place the new random region d base pairs downstream of the TSS of gene g; (4) if d is larger than the length of g then the random location is invalid, and we draw a new g.

For extragenic peaks the procedure is similar: (1) calculate the distance d to the nearest TSS (at position t); (2) select a gene g at random; (3) place the new random region at $t + d$; (4) ensure that the location is extragenic; if it is not, then we draw a new g.

When selecting random control regions for comparing the eRNA levels found at the putative enhancers, we wanted to control for the genomic location relative to TSSs as well as for the difficulty of mapping reads to repetitive regions. We defined m as the fraction of 35-mers in a given region that are unique to the mouse genome. For both extra- and intragenic, we also make sure that m is greater than 0.8 and we exclude the sites that do not fulfil this criterion.

Defining enhancers based on ChIP-Seq data. To locate enhancers, we started from the set of 41,148 CBP (Millipore) peaks located by our peak-finding algorithm. Supplementary Table 1 indicates the number of CBP peaks at each stage of this filtering. (We note that the analysis in the main text and main figures is primarily focused on the extragenic peaks.) To be considered as enhancers, individual CBP peaks had to meet the following criteria: (1) the CBP peak had to be replicated with the Abcam CBP antibody (see reproducibility section). (2) The CBP peak had to be at least 1 kb away from all annotated TSSs. (3) CBP peaks with abnormally high levels of both H3K4me1 and H3K4me3 enrichment in a 2-kb bin centred on the peak were also removed. There were 159 sites that were disallowed based on this criterion. When examined in the UCSC Genome browser, these sites showed unusually long (>500 bp) regions of very strong enrichment for multiple transcription factors, suggesting that they were not true binding sites. (4) On the basis of evidence from ESTs and other annotations, it is reasonable to suspect that some of the loci in our enhancer sites could correspond to true promoters. We wanted to take a conservative approach, and hence we removed all CBP peaks that have a 5′-sequenced EST from the UCSC Genome Browser spliced EST track that has a 5′ end within 2 kb of the CBP peak and that spans an annotated TSS. (5) We removed peaks that showed evidence of initiating long transcripts. We compared the regions −4 to −2 kb relative to the CBP peak with the region +2 to +4 kb on the forward strand. If the density in the downstream region was significantly higher than in the upstream region, we took this as evidence that a longer, possibly coding transcript was initiated at the loci. (6) An H3K4me1 peak had to be present within 2 kb in both replicates of stimulated H3K4me1. (7) The enrichment of H3K4me3 within a 2 kb window centred on the peak had to be less than 2 in both unstimulated and stimulated cells (Supplementary Fig. 8). (8) A very small number of CBP peaks (for example, those found near ribosomal RNA genes) had >10,000 RNA-Seq reads mapped within 1.5 kb. We removed these loci to simplify our analysis of RNA-Seq reads at enhancers.

Selection and clustering of enhancers. For each of the transcription factors CBP, CREB, NPAS4, SRF and RNAPII, the 1,000 enhancers with the highest levels of input-normalized ChIP-Seq reads within 200 bp of the enhancer centre were selected as well as the 1,000 enhancers with the highest levels of H3K4me1 within 1 kb. The enhancers were pooled and the ones without any divergent reads within 1.5 kb were removed. Subsequently, 315 enhancers were selected at random and ordered by row on the basis of k-means clustering performed in R, based on the transcription factors mentioned above, the amount of H3K4me1 and the amount of divergent RNA-Seq signal (Fig. 5a).

Directionality index. A directionality index used in Fig. 5b was defined as $|f - r|/(f + r)$, where f is the number of divergent reads on the forward strand and r is the number of divergent reads on the reverse strand within 1.5 kb of the CBP peak or TSS. The estimation of the directionality index is complicated by the fact that the number of reads found at enhancers is much smaller than the number of reads found at promoters. To make sure that the observed difference is not an artefact due to the lower levels of eRNAs, we down-sampled the number of reads at promoters to match the eRNA read numbers.

Detection of enhancers with eRNAs. As a negative control for the eRNAs, we compared with the adjacent regions −3.5 to −2 kb and +2 to +3.5 kb. A less stringent control is provided by the random control loci where we used the −1.5 to +1.5 kb regions. If one requires >7 reads for detection, 2,267 or 44% of the enhancers have eRNAs, compared to 16% of the flanking regions and 2% of the random regions (Fig. 5c).

For the intragenic enhancers, in examining eRNA transcription we were limited to considering the antisense strand. Using a similar strategy to that shown in Fig. 5c, we found that 22% of intragenic enhancers had more than four antisense reads within 1.5 kb of the CBP peak, whereas 14% of the enhancers had more than four antisense reads in the flanking regions.

Changes in eRNA levels and RNAPII binding at enhancers. For changes in RNAPII binding at enhancers, we counted the number of ChIP-Seq reads within 300 bp of the enhancer centre at each time point. For eRNAs, we used the same procedure, including all reads within 1.5 kb of the enhancer. We defined the normalized induction index as $(s - u)/(s + u)$, where s and u are the number of normalized reads from the stimulated and unstimulated conditions, respectively (Fig. 5d).

Correlations between enhancer features and mRNA expression levels at nearby genes. We paired each enhancer with the nearest TSS, provided that the distance was <1 Mb. The induction index for RefSeq genes was calculated as before for RNAPII, but based on the average read density throughout the coding region for mRNA. Genes were grouped by induction ratio quantiles into 25 bins before plotting (Fig. 5d).

Searching for known consensus motifs. For each enhancer and TSS where an NPAS4 peak was found we searched for perfect matches to the NPAS4 consensus motifs 'CACGC' and 'CACGTA'[37] on both strands in a 300-bp window centred around the CBP peak or the TSS. Surprisingly, at least one of the motifs was found in 66% of the promoter peaks but only in 27% of the peaks found at enhancers. The fraction of enhancers with the NPAS4 motifs is only marginally larger than the 22% found at TSSs lacking NPAS4 binding or the 14% found at random loci. Given the fact that there is no significant difference between the peak sizes found at enhancers and promoters (Supplementary Table 1), this result suggests that the mechanism of binding of NPAS4 to promoters and enhancers may differ, as has been observed for other factors.

Induced genes. We provide Supplementary Table 8, showing a list of KCl-regulated genes used for analysis in Fig. 5. The list was generated using our most deeply sequenced RNA-Seq experiment and filtered for fold-change and a z-score ensuring adequate read number. The list of genes is consistent with previous experiments published using array technologies[27,38], and is well correlated with replicate RNA-Seq experiments.

Gene ontology analysis using DAVID. To examine whether particular gene classes were enriched either for CREB binding at their promoters or for regulation by KCl, we took KCl-regulated (Supplementary Table 8) or CREB-bound genes and asked whether particular gene classes were enriched. The results obtained using the software DAVID[39,40] are in Supplementary Table 7 (CREB) and Supplementary Table 9 (KCl-regulated genes).

Additional bioinformatics. Analysis of aligned reads was performed with a combination of custom Perl, Java, R, and MATLAB scripts. Additional details are available upon request.

Note on plots. In the case of plots with RefSeq promoters aligned by their mRNA TSSs: in each case, promoters are aligned so that the positions +1 to +1,000 bp along the x axis correspond to the first 1 kb of each reference sequence annotated pre-mRNA, and the positions −1,000 to −1 bp consist of the first 1 kb upstream of each mRNA TSS. For plots with enhancers aligned at the centre of their CBP binding site, the same logic applies with the CBP peak centre substituting for the mRNA TSS. Owing to different sequencing depths, different scales are required in Figs 1 and 6a for displaying different ChIP results. For Fig. 1, the scales are H3K4me3 (0–1), H3K4me1 (0–1), H3K27me3 (0–1), SRF (0–3.5), CBP (0–3), CREB (0–2), NPAS4 (0–3), RNAPII (0–3), RNA-Seq (0–10), where the numbers in parentheses are normalized read counts. The corresponding numbers for Fig. 6a are H3K4me3 (0–0.5), H3K4me1 (0–2), SRF (0–7), CBP (0–1), RNAPII (0–1.8), RNA-Seq (0–10). Note that no input subtraction was performed for these plots. The conservation track shows 30-way Multiz alignment and conservation scores (PhastCons).

27. Kawashima, T. *et al.* Synaptic activity-responsive element in the Arc/Arg3.1 promoter essential for synapse-to-nucleus signaling in activated neurons. *Proc. Natl Acad. Sci. USA* 106, 316–321 (2009).

28. Couttlet, P. *et al.* Messenger RNA deadenylation precedes decapping in mammalian cells. *Proc. Natl Acad. Sci. USA* **94**, 5628–5633 (1997).

29. Flavell, S. W. *et al.* Genome-wide analysis of MEF2 transcriptional program reveals synaptic target genes and neuronal activity-dependent polyadenylation site selection. *Neuron* **60**, 1022–1038 (2008).

30. Kharchenko, P. V., Tolstorukov, M. Y. & Park, P. J. Design and analysis of ChIP-seq experiments for DNA-binding proteins. *Nature Biotechnol.* **26**, 1351–1359 (2008).

31. Rozowsky, J. *et al.* PeakSeq enables systematic scoring of ChIP-seq experiments relative to controls. *Nature Biotechnol.* **27**, 66–75 (2009).

32. Robertson, A. G. *et al.* Genome-wide relationship between histone H3 lysine 4 mono- and tri-methylation and transcription factor binding. *Genome Res.* **18**, 1906–1917 (2008).

33. Skellam, J. G. The frequency distribution of the difference between two Poisson variates belonging to different populations. *J. R. Stat. Soc. A* **109**, 296 (1946).

34. Efron, B. Microarrays, empirical Bayes and the two-groups model. *Stat. Sci.* **23**, 1–22 (2008).

35. Benjamini, Y. & Hochberg, Y. Controlling the false discovery rate: a practical and powerful approach to multiple testing. *J. Roy. Statist. Soc. Ser. B. Methodol.* **57**, 289–300 (1995).

36. Jothi, R., Cuddapah, S., Barski, A., Cui, K. & Zhao, K. Genome-wide identification of *in vivo* protein–DNA binding sites from ChIP-Seq data. *Nucleic Acids Res.* **36**, 5221–5231 (2008).

37. Ooe, N. *et al.* Identification of a novel basic helix-loop-helix-PAS factor, NXF, reveals a Sim2 competitive, positive regulatory role in dendritic-cytoskeleton modulator drebrin gene expression. *Mol. Cell. Biol.* **24**, 608–616 (2004).

38. Lin, Y. *et al.* Activity-dependent regulation of inhibitory synapse development by Npas4. *Nature* **455**, 1198–1204 (2008).

39. Huang, D. W., Sherman, B. T. & Lempicki, R. A. Systematic and integrative analysis of large gene lists using DAVID Bioinformatics Resources. *Nature Protocols* **4**, 44–57 (2009).

40. Dennis, G. Jr *et al.* DAVID: Database for Annotation, Visualization, and Integrated Discovery. *Genome Biol.* **4**, 3 (2003).